Fuel 287 (2021) 119463

Contents lists available at ScienceDirect

Fuel

journal homepage: www.elsevier.com/locate/fuel

Full Length Article

Flower-like δ-MnO_2 as cathode material of Li-ion batteries of high charge-discharge rates

Y.Y. Rivera-Lugo [a], R.M. Félix-Navarro [a], B. Trujillo-Navarrete [a], E.A. Reynoso-Soto [a], C. Silva-Carrillo [a], C.A. Cruz-Gutiérrez [a], E. Quiroga-González [b], J.C. Calva-Yáñez [c,*]

[a] Tecnológico Nacional de México/Instituto Tecnológico de Tijuana, Centro de Graduados e Investigación en Química, Blvd. Industrial, S/N, Otay Tecnológico, 22500 Tijuana, BC, Mexico

[b] Institute of Physics, Benemérita Universidad Autónoma de Puebla, 72570 Puebla, Mexico

[c] CONACYT-Tecnológico Nacional de México/Instituto Tecnológico de Tijuana, Centro de Graduados e Investigación en Química, Blvd. Industrial, S/N, Otay Tecnológico, 22500 Tijuana, BC, Mexico

A B S T R A C T

Cathodes of lithium-ion batteries (LIBs) present stability and performance issues, therefore, the search of new cathodes is still a major concern. Manganese dioxide in delta phase (δ-MnO_2) seems to be a suitable candidate since is low-cost, non-toxic and possesses a theoretical capacity of 308 $mAhg^{-1}$ for one-electron transfer. In this work, we prepared δ-MnO_2 by a hydrothermal method at two different reaction times. At 2 h, a flower-like nanostructure was obtained, while for a 3 h reaction time, a solid nanostructure was achieved. Both materials were tested as cathode in a LIB, finding that at slow charge-discharge rates (20 mAg^{-1}), a material with homogeneous nanosized morphology is enough in order to obtain good capacities. But, at higher rates, our flower-like structure provides a better discharge capacity.

1. Introduction

Lithium-ion batteries (LIBs) possess a high storage capacity that allows their application in almost every electric device, from cellphones to vehicles [1,2]. Commercially, there are three cathodes types: Li_xMnO_2 (M = Co, Ni, Mn), LiM_2O_4 (M = Co, Ni, Mn) and $LiMPO_4$ (M = Fe) [3]. However, due to stability and performance issues (low capacity, structural changes, among others) these are non-suitable cathodes anymore [4]. Manganese dioxide (MnO_2) is low-cost and non-toxic material that could present various crystal structures that allow intercalation of cations, which makes it a promising electrode material for energy storage applications [5–8].

MnO_2 can be found as α-MnO_2, β-MnO_2, γ-MnO_2, ε-MnO_2 and δ-MnO_2, presenting different crystal structures. The most studied material for Li-ion batteries, due to its good reversibility, is α-MnO_2 [9]; however, bulk MnO_2 capacity decays rapidly due to volume changes, which leads to the transformation of the crystalline structure [10]. In order to overcome this situation, nanomaterials have been proposed, since they provide a large surface, which assures a better contact between electrode and electrolyte, shorting Li^+ pathways [11–13]. Also, δ-MnO_2 is capturing much attention due to its theoretical capacity of 308 $mAhg^{-1}$, which has allowed its application in energy storage in different types of batteries [14–19]. It has a lamellar structure of MnO_6 octahedral sheets that share edges, and interlayers can intercalate ions of 7 Å or less, like Li^+ [20], which is an advantage in its use within lithium-ion batteries, since the Li-ion does not return to the same place where it was extracted, so when returning to the cathode and reincorporating in another area prevents changes in volume, reducing the risk of material pulverization and, therefore, improving the stability of the cathode. Different crystalline structures of MnO_2 have been tested as cathodes in LIBs, for example, Wang et al., synthesized δ-MnO_2 and tested it as a cathode in a LIB battery, where they discover that the material exhibited poor cycling stability, showing an initial value of 138 $mAhg^{-1}$, decaying at 71 and 29 at cycles 50th and 100th [21]. Moazzen et al., prepared MnO_2 nanoparticles consisting of ramsdelite (R-MnO_2) and akhtenskite (ε-MnO_2) polymorphs (37:63 wt%), where they found that the initial 278 $mAhg^{-1}$ discharge capacity rapidly faded [22]. However, during our research we discover that there are few papers that studied charge-discharge tests at high rates (>1000 mAg^{-1}). Pol et al., studied α-MnO_2 at different rates, including 500 mAg^{-1}, obtaining a low specific capacity of less than 50 $mAhg^{-1}$, which was associated to the sluggish kinetics of Li ion at high current density [23]. Wang et al., prepared δ-MnO_2 and tested it as cathode in a LIB, showing a discharge capacity of 23 mAg^{-1} at 1540 mAg^{-1}, but the size of their material was about 200–300 nm. Also, the binding and conductive agents that they employed were Super P and CMC 4% [21]. In this work, we synthesized

* Corresponding author.
E-mail address: jccalva@conacyt.mx (J.C. Calva-Yáñez).

https://doi.org/10.1016/j.fuel.2020.119463
Received 6 March 2020; Received in revised form 1 October 2020; Accepted 7 October 2020
Available online 27 October 2020

δ-MnO_2 of 150 nm by a hydrothermal method, varying the reaction time: 2 and 3 h, where δ-MnO_2,2h had a flower-like structure and δ-MnO_2,3h presented solid spheres. These materials were tested as a cathode in a Li-ion battery, where it was possible to determine that at slow rates, a material with homogeneous nanosized morphology is enough in order to obtain good capacities. However, for the rest of rates, especially high rates, the flower-like structure of δ-MnO_2,2h presented better charge–discharge capacities of 44 and 24 $mAhg^{-1}$ at 1000 and 2000 mAg^{-1}, respectively.

2. Experimental

All chemicals reagents received without further purification. Polyvinylidene fluoride (PVDF), 1-methyl-2-pyrrolidinone (NMP) and lithium hexafluorophosphate in ethylene carbonate and diethyl carbonate ($LiPF_6$/EC/DEC (50/50)) were acquired from Sigma-Aldrich. Potassium permanganate ($KMnO_4$, 98%), carbon black, manganese (II) sulfate ($MnSO_4{\cdot}H_2O$, 100%), acetone (CH_3COCH_3, 99.5%) and Celgard 2400 membranes were purchased from Alfa-Aesar, Fuel Cell Store®, Fermont, Faga Lab and Asahi Kasei, respectively. All aqueous solutions were prepared with Milli-Q® water (18 MΩ, Millipore).

2.1. Synthesis of δ-MnO_2.

The synthesis of δ-MnO_2 was carried out through a hydrothermal method [24]. Briefly, 1.8 mmols of $KMnO_4$ were placed in 25 mL of water and allowed to stir for 15 min. Simultaneously, 0.3 mmol of $MnSO_4$ in 25 mL of water was stirred. After, both solutions were mixed in a Teflon reactor for 30 min. Then, the mixture was placed in a stainless-steel reactor and the reaction proceeded for 2 or 3 h at 160 °C. Finally, the product was collected, centrifuged (5000 rpm for 15 min) and washed three times with water and acetone. The reaction is in Equation (1).

$$2KMnO_4 + 3MnSO_4 + 2H_2O \rightarrow 5MnO_2 + K_2SO_4 + 2H_2SO_4 \quad (1)$$

2.2. Physicochemical and electrochemical characterization

The identification of crystalline phases was performed by X-ray diffraction (XRD) employing a diffractometer Philips X'pert MPD. The intensity data were collected with 2θ ranging from 3 to 90° with 0.05° of step-size. The morphology of MnO_2 was analyzed by scanning electron microscopy (Tescan, Vega3). The specific surface area was obtained by an Autosorb-iQ (Quantachrome Instruments) using the Brunauer-Emmet-Teller (B.E.T.) equation. A potentiostat/galvanostat (Biologic, VMP-300) was used for all the electrochemical tests. An El Cell-cell battery was employed at room temperature (25 ± 1 °C), were ($LiPF_6$/EC/DEC (50/50) and Celgard 2400 were used as an electrolyte and as a separator membrane, respectively, and the cathodes were stainless steel disks (d = 17 mm). Catalytic inks were prepared, containing 80 wt% of MnO_2, 10 wt% of PVDF, 10 wt% of carbon black and N-mp (N-methyl-pyrrolidone) was used as a solvent. The ink was used to modify the surface of the cathodes. One modified, the cathode was placed on a heating grid for 60 min at 250 °C with a heating ramp of 25 °C/min. For the LIB assembly, a sandwich structure was followed, placing the cathode first, then the membrane and, finally, the lithium chip. Before assembly, the membrane was immersed in the electrolyte ($LiPF_6$/EC/DEC (50/50)) for 4 h. In all measurements, a lithium chip was employed as the anode and a glove box with controlled Ar environment was used for the LIB assembly. Cyclic voltammograms (CV) were carried out in the potential range from 2.0 to 4.5 V vs. Li/Li^+ at a scan rate of 0.1 mVs^{-1}. Electrochemical impedance spectroscopy (EIS) was evaluated in the frequency range from 10 mHz to 100 kHz. The charge-discharge curves were studied through battery capacity determination (BCD) analysis, in the same potential range as CV.

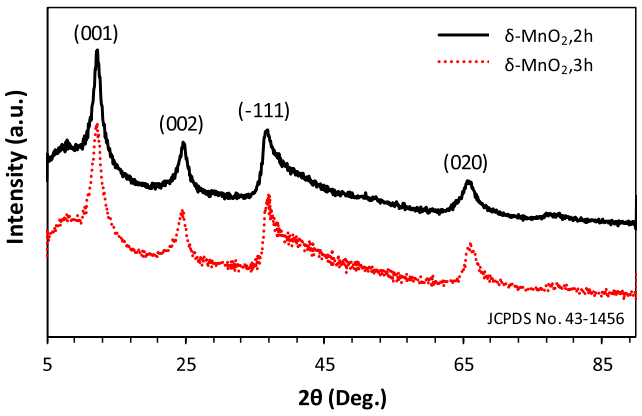

Fig. 1. X-ray diffraction patterns of flower like δ-MnO_2 synthesized in 2 h and 3 h.

3. Results AND discussion

3.1. Physicochemical characterization

Fig. 1 shows XRD spectra of flower like δ-MnO_2 synthesized at 2 h and 3 h. In both materials, diffraction peaks at 12.2, 24.8, 37 and 66° of 2θ were obtained, corresponding to crystalline planes (001), (002), (−111) and (020), respectively, of δ phase (JCPDS No. 43-156). Peaks corresponding to other MnO_2 phases were not observed, which confirm

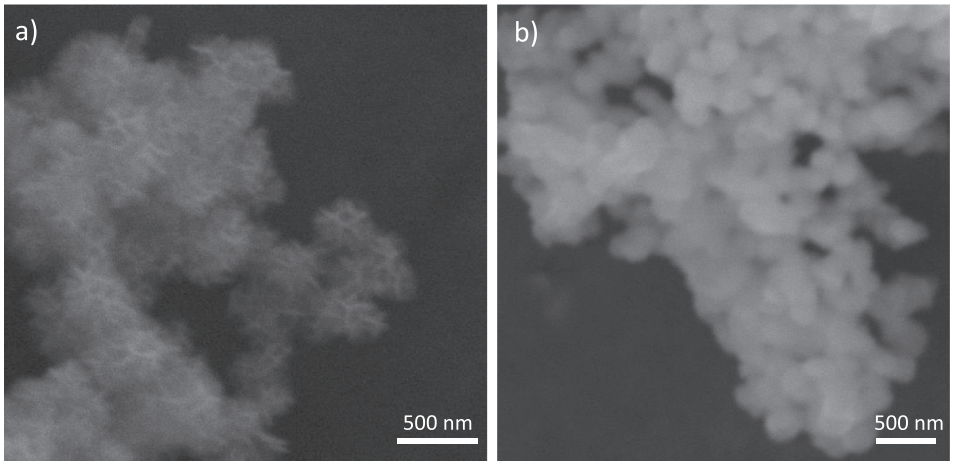

Fig. 2. SEM micrographs of flower like δ-MnO_2 at different synthesis time. a) 2 h and b) 3 h.

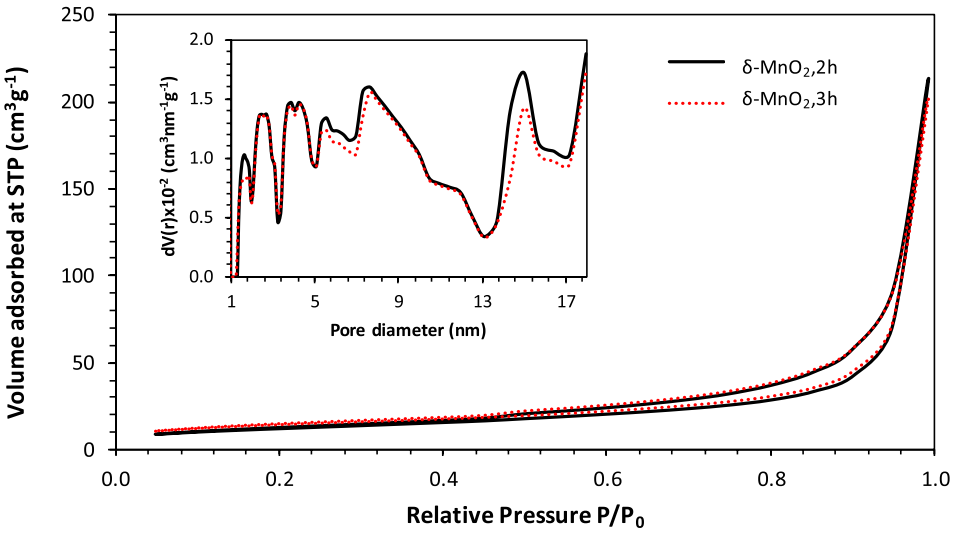

Fig. 3. N_2 adsorption-desorption isotherms and pore size distribution (inset image) of flower like δ-MnO_2 synthesized at 2 and 3 h.

the purity of the material. The δ-MnO_2 is made up from loosely bound layers of edge shared MnO_6 located at the (0 0 1) planes. Its crystal structure is birnessite (monoclinic). The lattice constants for δ-MnO_2,2h, are a = 0.5147 nm, b = 0.2834 nm and c = 0.7193 nm (spacing between (0 0 1) planes), while a = 0.5136 nm, b = 0.2828 nm and c = 0.7252 nm for δ-MnO_2,3h. c corresponds to the spacing between MnO_6 monolayers [24]. From these results, we obtained the c/b value (an indication of anisotropical growth in the axial direction), being 2.538 for δ-MnO_2,2h, and 2.564 for δ-MnO_2,3h. Correlating this parameter with the synthesis time, one could infer that the crystallites elongate in the c axis as a function of the synthesis time due to the insertion of a larger number of free K^+ cations into the interlayer spacing.

The method to determine the apparent density of a flower-like δ-MnO_2 sample is the same method for determining the bulk density of any powder. In case of a monoclinic structure, the volume of unit cell is determined as:

$$V = abc^{*}\sin(\beta) \tag{2}$$

For our birnessite monoclinic type structure β = 103.7° for δ-MnO_2,2h and 103.8° δ-MnO_2,3h, and the unit cell is made up of four bases for a total of two atoms of Mn and 6 atoms of O. The density of the material is calculated as:

$$\rho = \frac{M}{V} = \frac{[(15.998^{*}6) + (54.938^{*}2)]}{abc\sin(\beta)^{*}6.023^{*}10^{23}} \tag{3}$$

where M is the molar mass and V is the volume of the unit cell.

Then, the value of density is determined as: 3.353×10^6 g m^{-3} and 3.341×10^6 g m^{-3} for δ-MnO_2,2h and δ-MnO_2,3h respectively, which corresponds to data reported in specialized literature.

Morphology and size of δ-MnO_2 were studied by SEM, as can be seen in Fig. 2. δ-MnO_2,2h showed homogeneous particles in a structured order. These particles, of about 150 nm, presented a flower-like morphology and, accordingly to Yu et al., these flower-like structures are composed of interconnected nanosheets that forms the 3-D structured [25]. Semi-homogeneous particles in a structured order were able to see in δ-MnO_2,3h (Fig. 2b). However, the flower-like structure was not present. Based on SEM results, we can propose that in this hydrothermal reaction, as the reaction time pass, the flower-like structure gets lost, which can be because the nanosheets experiment an Ostwald ripening, forming a solid structure at the reaction time of 3 h.

Textural properties of nanomaterials are a measure of available space or total volume that would be occupied by Ions or molecules in reactions and mass transfer processes, in the specific case of batteries, this space could be occupied by Li ions. Nitrogen adsorption/desorption isotherms of mesoporous flower like δ-MnO_2 samples synthesized at 2 and 3 h are provided in Fig. 3, which are typical IV type pattern with H_3

Table 1
Specific surface area, and pore size of flower like δ-MnO_2 synthesized at 2 and 3 h.

Sample	Surface area (m^2 g^{-1})	Half pore width (nm)
δ-MnO_2,2h	43.601	18
δ-MnO_2,3h	38.547	18

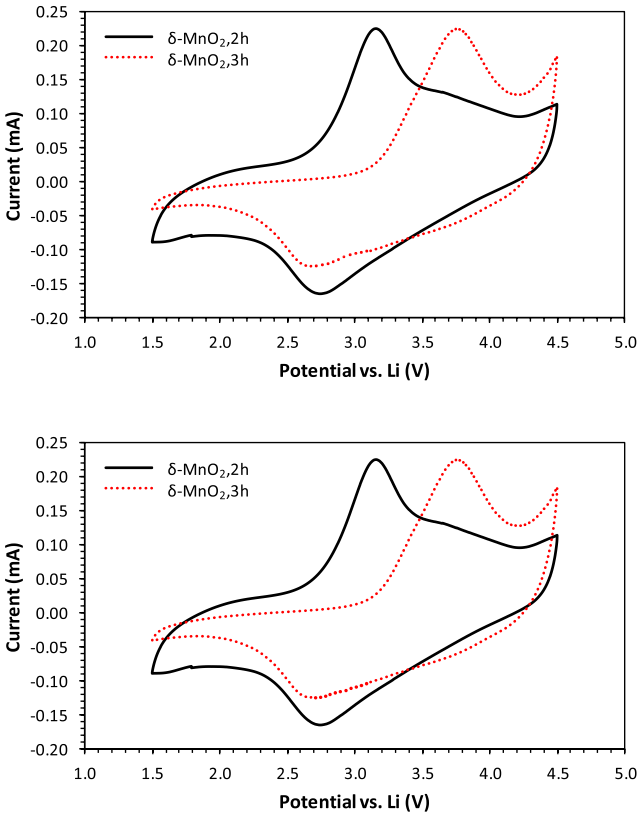

Fig. 4. Cyclic voltammograms of Li^+ battery cathodes based on flower like δ-MnO_2 synthesized at 2 h and 3 h.

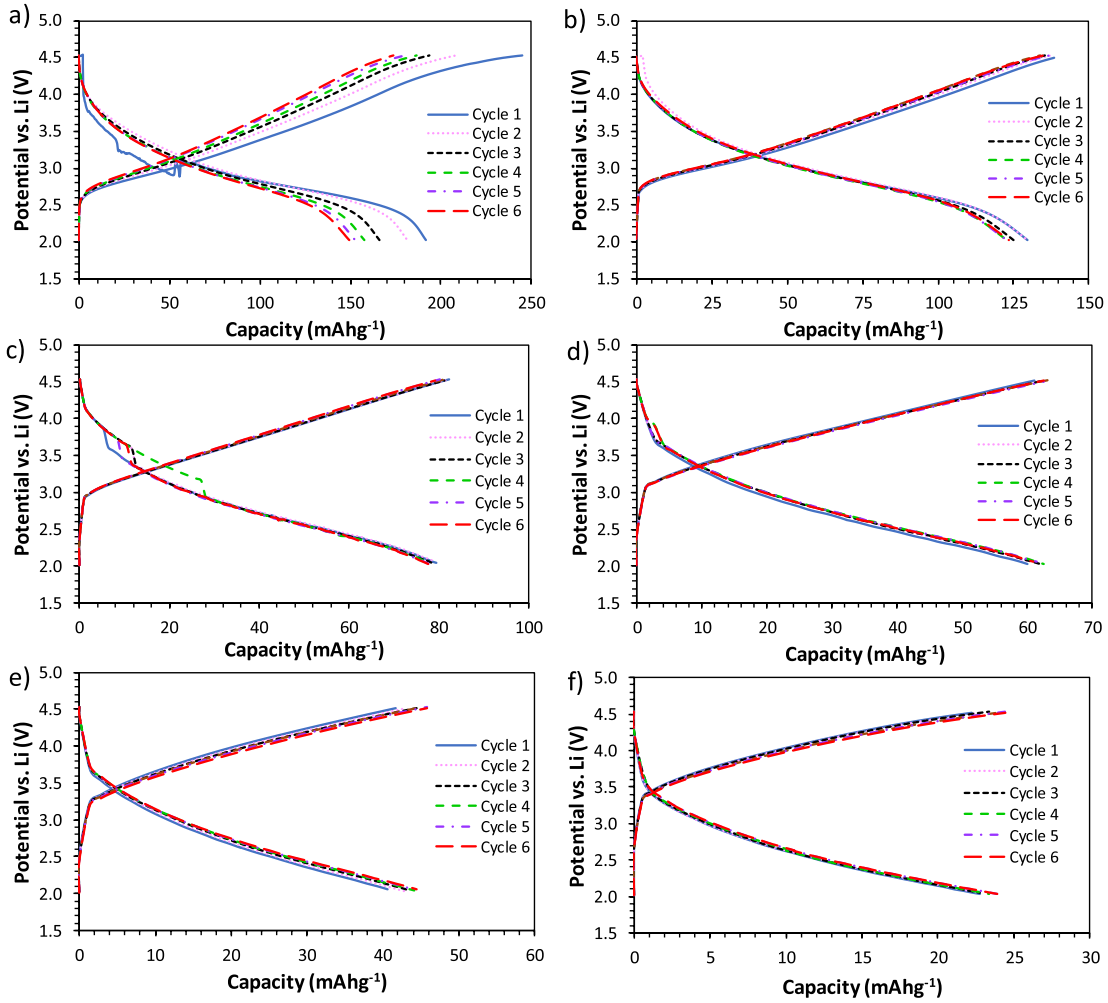

Fig. 5. Charge-discharge performance of flower like δ-MnO_2,2h at a) 20, b) 50, c) 250, d) 500, e) 1000 and f) 2000 mAg^{-1}.

hysteretic loops in the range of 0.5–0.95P/P_0, indicating the existence of complex pore structures with networking significant effects, where adsorption metastability and desorption branch delayed by phenomena as pore blocking and cavitation associated with pore evaporation in networked structures (ink-bottle pores). A complete pore size distribution can only be obtained using a statistical mechanics-based approach which correctly accounts for delayed condensation on the adsorption branch [26]. N_2 at 77 K on carbon (slit pore NLDFT equilibrium model) DFT method was used to determine the pore size distribution and surface area, its observed that the average pore size distribution is in the range of 2–17 nm, following both materials a similar distribution. As expected, our flower-like structure (δ-MnO_2,2h) showed a larger surface area than the compact structure (δ-MnO_2,3h) The results are summarized in Table 1.

3.2. Electrochemical characterization

Cyclic voltammetry (CV) was employed to determine the oxidation/reduction peaks of Mn^{4+}→Mn^{3+}, by the insertion/extraction of Li^+. Fig. 4 shows the 4th cycle for flower like δ-MnO_2,2h and δ-MnO_2,3h cathodes, where it can be seen that for δ-MnO_2,2h the oxidation peak is presented at 3.10 V while for δ-MnO_2,3h this peak is visible at 3.77 V. In both materials, the reduction is peak is observed at 2.68 V. The chemical reactions involved in the charge and discharge processes of MnO_2 when used as cathode in a LIB are described in equation (2) [27,28].

$$xLi^+ + MnO_2 \underset{Discharge}{\overset{Charge}{\rightleftarrows}} Li_x(Mn)_x^{3+}(Mn)_{1-x}^{4+}O_2 \quad (4)$$

A maximum of one Li^+ ion could be allocated per unit of MnO_2, which makes a theoretical capacity of 308 mAh g^{-1}.

Reversible reactions are expected in CV, because they indicate that the cathode can receive the Li^+ and can also give it back to the anode electrode. It is also noticeable that δ-MnO_2,2h had a more reversible lithiation/de-lithiation that δ-MnO_2,3h due to the smallest ΔV. Based on CV results, we expect both of our materials to respond well to the charge–discharge tests. It is important to consider that the faradaic events occur at the voltammetric peaks. The base-current is capacitive-like (displacement current). Calculating the areas under the peaks, we can see that they are larger for the sample of 3 h. However, the area of the displacement current is larger for the sample of 2 h. This perfectly explains why at slow charge/discharge rates the capacity is larger for δ-MnO_2,3h, while at high rates it is larger for δ-MnO_2,2h.

It was performed 6 cycles of charge-discharge tests for δ-MnO_2,2h cathodes, showing the obtained results in Fig. 5. At 20 mAg^{-1}, a rapid capacity loss of 22% was observed. However, as the cycles passed, the capacity loss decreased at 5% at 50 mAg^{-1}, and at 250, 500, 1000 and 2000 mAg^{-1} it remains unchanged. This means that our flower-like structure it is not stable at slow rates but at higher rates, even at 2000 mAg^{-1}, it provides a stable cycling. Charge-discharge profiles of

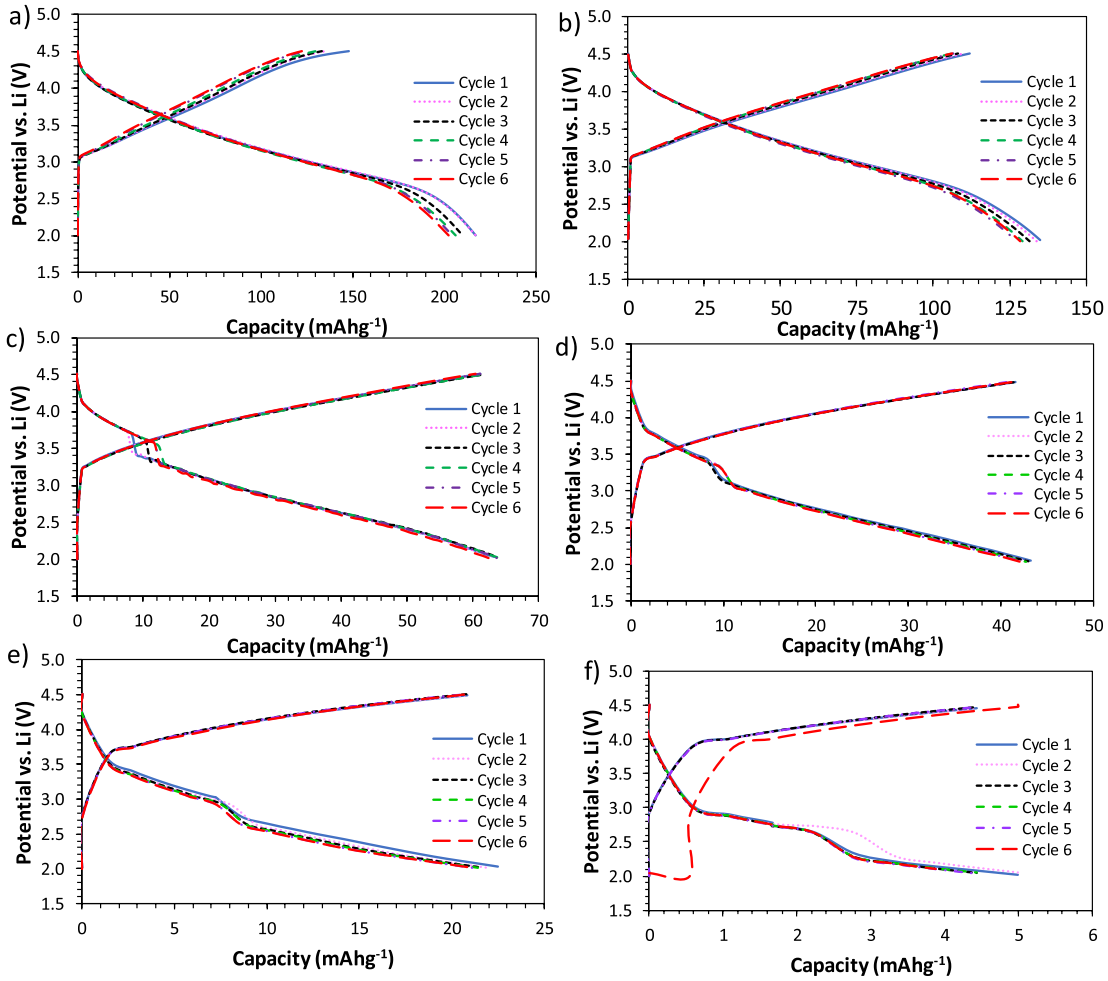

Fig. 6. Charge-discharge performance of flower like δ-MnO_2,3h at a) 20, b) 50, c) 250, d) 500, e) 1000 and f) 2000 mAg^{-1}.

δ-MnO_2,3h for 6 cycles at different rates are shown in Fig. 6. δ-MnO_2,3h showed a discharge capacity loss of around 5% for the slowest rates (20 and 50 mAg^{-1}). From 250 to 1000 mAg^{-1}, the capacity seems unchanged and, finally, for 2000 mAg^{-1}, the initial capacity decays almost 10%. The capacity loss through cycling has been previously observed and can be associated to the partial irreversibility of the lithiation in the first cycle [29–31]. Also, *δ-MnO*$_2$,3h showed two-staged voltage plateaus when studied between 250 mAg^{-1} and 2000 mAg^{-1}, which could be caused by a slight polarization due to the increased charge-discharge rates [32]. The latest behavior is not presented in δ-MnO_2,2h sample, which has shown a better performance and stability at high charge-discharge rates. In both materials, it was possible to observe a gradual decrease in capacity as the discharge rate increased, which indicates a kinetic process controlled by the diffusion of Li^+ [33]. It is also noticeable that different charge-discharge capacities values were obtained at the beginning of tests, which can be because after the first cycles a nanoporous structure is formed in the cathodes, which facilitates the penetration of the electrolyte into the nanopores of the electrode [34], allowing a better flow of electrons and lithium ions in subsequent cycles, obtaining very similar values for charging and discharging [35]. At low charge/discharge rates, the charge storage mechanism is basically intercalation. It is the most common mechanism in layered metal oxides. However, at high charge/discharge rates the Li ions may intercalate not so deep into the material, being the intercalation depth closer to the surface when the rates are faster. In this way, as the material MnO_2,2h presents larger surface areas, it presents higher capacities at high rates.

It is important to mention that although the electrochemical performance of our materials is not as good compared to previously reported materials at low charge/ discharge rates, one of them has a better performance at fast charge/discharge regimes. It should be noted that the reported materials used conductive additives to improve their performance (e.g. adding graphene). The idea of our report is to present a material that without the use of any special additive such as graphene, one can accomplish high rates.

From Fig. 7, it can be observed that δ-MnO_2,3h had a better capacity discharge that δ-MnO_2,2h for 20 and 50 mAg^{-1}, the slowest rates studied. However, in the rest of the rates δ-MnO_2,2h had superior performance, which from the best of our knowledge there are no bare MnO_2

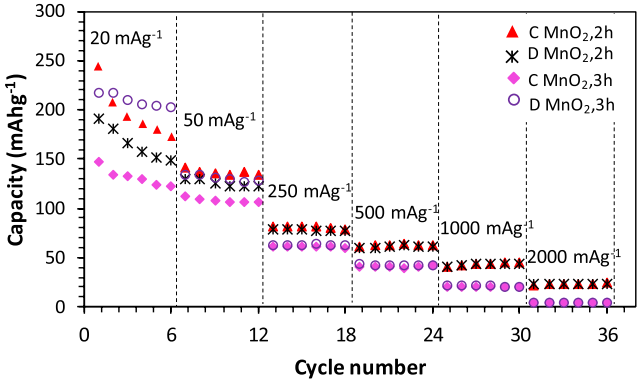

Fig. 7. Rate capability performance of Li^+ battery cathodes based on δ-MnO_2,2h and δ-MnO_2,3h.

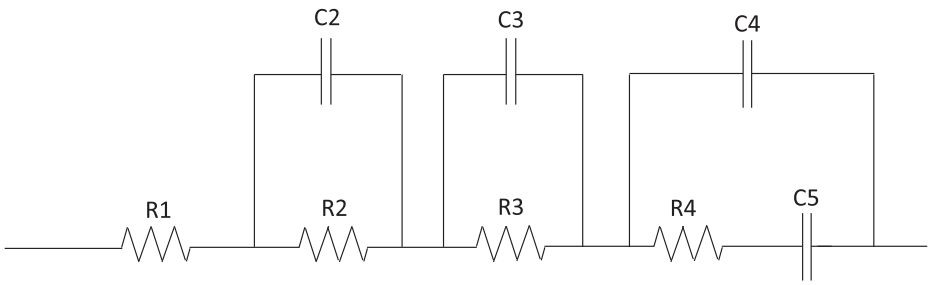

Fig. 8. Equivalent circuit used for the fitting of the impedance data.

cathodes published that can improve the obtained values for δ-MnO_2,2h at 2000 mAg^{-1}. From this, we can say that for a really slow process (20 mAg^{-1}), a material with homogeneous nano-sized morphology is enough in order to obtain good capacities. However, for the rest of rates, especially high rates, the flower-like structure of δ-MnO_2,2h seems to provide a better contact area between electrode and electrolyte. Besides, this material had a larger specific area, facilitating the Li^+ transport, therefore, showing good discharge capacities.

There are four frequency regions in the impedance of the half battery cells prepared with the two materials of this work, agreeing with other works of cathodes and anodes of Li-ion batteries [36,37]: region A, corresponding to battery Ohmic losses; high-frequency region B related to the transport in the electrolyte; medium frequency region C, of interfaces caused by decomposition products (called solid electrolyte interface – SEI–, more common for anodes) resistance; and low-frequency region D, caused by charge transfer to the active material, and by diffusion inside this material (represented by a Warburg element Z_w). The equivalent circuit used to model the impedance of the batteries is shown in Fig. 8. Every frequency region is modeled by an R/C circuit. R1 is related to region A, R2/C2 to region B, R3/C3 to region C, and C4/(R4 + C4) to region D. In particular C4 is the capacitive effect caused by charge transfer, and C5 models the diffusion to the active material.

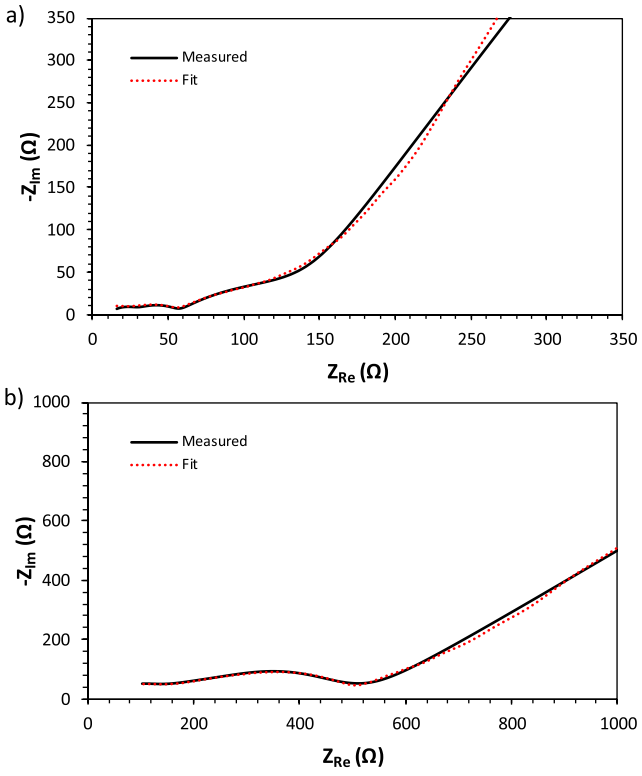

Fig. 9. a) Impedance spectrum of half battery cell using flower like δ-MnO_2 synthesized in 2 h as cathode, and b) impedance spectrum of half battery cell using compact flower like δ-MnO_2 synthesized in 3 h as cathode.

Fig. 9a) shows the impedance spectrum of a battery with the material prepared in 2 h, while Fig. 9b) shows the impedance spectrum of the sample prepared in 3 h, after being cycled for 48 cycles with different charge/discharge energy density values, from 20 to 2000 mAg^{-1}. A fit using the equivalent circuit of Fig. 8 was performed. As can be observed in the figures, the fitted curve agrees well with the measured data. At a first glance, it is possible to see that the total impedance for the sample of 3 h is larger than 2 h. From the values of the fitted variables, it is possible to see, in particular, that R4 (the charge transfer resistance) is of 129 O for the sample δ-MnO_2,2h, and it is of 404 O for the sample δ-MnO_2,3h. Having a larger resistance may produce that the voltage limits during the charge/discharge cycles are reached faster, enabling just lower capacities.

4. Conclusions

The synthesis of δ-MnO_2 at 2 and 3 h were carried out successfully, where MnO_2,2h showed homogeneous flower like nanoparticles in a structured order and δ-MnO_2,3h had semi-homogeneous more compact flower like nanoparticles in a structured order. These materials were used as a cathode in a Li-ion battery at different charge–discharge rates, discovering that at slow rates, a material with homogeneous nanosized morphology is enough in order to obtain good capacities, but at high rates, a flower-like nanostructure provides better results, with data of 24 $mAhg^{-1}$ at 2000 mAg^{-1}.

CRediT authorship contribution statement

Y.Y. Rivera-Lugo: Data curation, Formal analysis, Investigation, Methodology, Writing - original draft. **R.M. Félix-Navarro:** Supervision, Data curation, Formal analysis, Software, Funding acquisition, Project administration, Resources. **B. Trujillo-Navarrete:** Supervision, Data curation, Formal analysis, Writing - review & editing. **E.A. Reynoso-Soto:** Supervision, Data curation, Software. **C. Silva-Carrillo:** Data curation, Formal analysis, Methodology. **C.A. Cruz-Gutiérrez:** Data curation, Formal analysis, Methodology. **E. Quiroga-González:** Supervision, Data curation, Formal analysis, Writing - review & editing. **J.C. Calva-Yáñez:** Conceptualization, Supervision, Formal analysis, Project administration, Writing - original draft.

Declaration of Competing Interest

The authors declare that they have no known competing financial interests or personal relationships that could have appeared to influence the work reported in this paper.

Acknowledgments

This work was financially supported by SENER-CONACyT of Mexico under grant 292862. Y. Y. Rivera-Lugo would like to thank to CONACyT

for the scholarship provided for her doctorate science research (scholar fellow 328834). The authors would like to thank to Dr. Sergio Pérez Sicairos for providing some materials for the experiments, and Martha Eloisa Aparicio Ceja for the XRD measurements.

References

[1] Cameán I, Lavela P, Tirado JL, García AB. On the electrochemical performance of anthracite-based graphite materials as anodes in lithium-ion batteries. Fuel 2010; 89:986–91. https://doi.org/10.1016/j.fuel.2009.06.034.
[2] Zhang Y, Zhang K, Jia K, Liu G, Ren S, Li K, Long X, Li M, Qiu J. Preparation of coal-based graphene quantum dots/α-Fe_2O_3 nanocomposites and their lithium-ion storage properties. Fuel 2019;241:646–52. https://doi.org/10.1016/j.fuel.2018.12.030.
[3] van Schalkwijk WA, Scrosati B. Advances in Lithium-Ion Batteries. New York: Kluwer Academic/Plenum Publishers; 2002. p. 3.
[4] Barghamadi M, Kapoor A, Wen C. A review on Li-S batteries as a high efficiency rechargeable lithium battery. J Electrochem Soc 2013;160:A1256–63. https://doi.org/10.1149/2.096308jes.
[5] Brock SL, Duan N, Tian ZR, Giraldo O, Zhou H, Suib SL. A Review of Porous Manganese Oxide Materials. Chem Mater 1998;10:2619–28. https://doi.org/10.1021/cm980227h.
[6] Wang J, Wang J-G, Qin X, Wang Y, You Z, Liu H, Shao M. Superfine MnO 2 nanowires with rich defects toward boosted zinc ion storage performance. ACS Appl Mater Interfaces 2020;12(31):34949–58. https://doi.org/10.1021/acsami.0c08812.
[7] Wang J, Wang J-G, Liu H, Wei C, Kang F. Zinc ion stabilized MnO 2 nanospheres for high capacity and long lifespan aqueous zinc-ion batteries. J Mater Chem A 2019;7: 13727–35. https://doi.org/10.1039/c9ta03541a.
[8] Li H, Wang H, Yang M, Sun Y, Yin Y, Guo P. Mg-inserted δ-MnO_2 nanosheet assembly for enhanced energy storage. Colloids Surf, A 2020;602:125068. https://doi.org/10.1016/j.colsurfa.2020.125068.
[9] Hashem AMA, Mohamed HA, Bahloul A, Eid AE, Julien CM. Thermal stabilization of tin- and cobalt-doped manganese dioxide. Ionics 2008;14(1):7–14. https://doi.org/10.1007/s11581-007-0138-3.
[10] Jiao F, Bruce PG. Mesoporous Crystalline β-MnO2—a Reversible Positive Electrode for Rechargeable Lithium Batteries. Adv Mater 2007;19(5):657–60.
[11] Kobayashi S, Kottegoda IRM, Uchimoto Y, Wakihara M. XANES and EXAFS analysis of nano-size manganese dioxide as a cathode material for lithium-ion batteries. J Mater Chem 2014;14:1843–8. https://doi.org/10.1039/B315443B.
[12] Kim IY, Ha H-W, Kim TW, Paik Y, Choy J-H, Hwang S-J. Origin of improved electrochemical activity of β-MnO 2 nanorods: effect of the mn valence in the precursor on the crystal structure and electrode activity of manganates. J Phys Chem C 2009;113(51):21274–82.
[13] Cheng F, Zhao J, Song W, Li C, Ma H, Chen J, Shen P. Facile controlled synthesis of MnO 2 nanostructures of novel shapes and their application in batteries. Inorg Chem 2006;45(5):2038–44.
[14] Peng H, Fan H, Yang C, Tian Y, Wang C, Sui J. Ultrathin δ-MnO 2 nanoflakes with Na + intercalation as a high-capacity cathode for aqueous zinc-ion batteries. RSC Adv 2020;10:17702–12. https://doi.org/10.1039/D0RA02556A.
[15] Raheem ZH, Sammarraie AMA. Synthesis of different manganese dioxide nanostructures and studding the enhancement of their electrochemical behavior in zinc-MnO_2 rechargeable batteries by doping with copper. AIP Conf Proc 2020; 2213:020187. https://doi.org/10.1063/5.0000246.
[16] Jiang Y, Ba D, Li Y, Liu J. Noninterference revealing of "layered to layered" zinc storage mechanism of δ-MnO 2 toward neutral Zn–Mn batteries with superior performance. Adv Sci 2020;7(6):1902795. https://doi.org/10.1002/advs.v7.610.1002/advs.201902795.
[17] Wang M, Yagi S. Layered birnessite MnO_2 with enlarged interlayer spacing for fast Mg-ion storage. J Alloy Compd 2020;820:153135. https://doi.org/10.1016/j.jallcom.2019.153135.
[18] Guo C, Liu HM, Li JF, Hou ZG, Liang JW, Zhou J, et al. Ultrathin delta-MnO_2 nanosheets as cathode for aqueous rechargeable zinc ion battery. Electrochim Acta 2019;304:370–7. https://doi.org/10.1016/j.electacta.2019.03.008.
[19] Ma L, Meng N, Zhang Y, Lian F. Improved electrocatalytic activity of δ-MnO_2@ MWCNTs by inducing the oriented growth of oxygen reduction products in Li-O2 batteries. Nano Energy 2019;58:508–16. https://doi.org/10.1016/j.nanoen.2019.01.089.
[20] Julien C, Massot M, Baddour-Hadjean R, Franger S, Bach S, Pereira-Ramos JP. Raman spectra of birnessite manganese dioxides. Solid State Ion 2003;159:345–56. https://doi.org/10.1016/S0167-2738(03)00035-3.
[21] Luo S, Xu S, Zhang Y, Liu J, Wang S, He P. Preparation of MnO_2 and MnO_2/carbon nanotubes nanocomposites with improved electrochemical performance for lithium ion batteries. J Solid State Electrochem 2016;20(7):2045–53. https://doi.org/10.1007/s10008-016-3208-5.
[22] Moazzen E, Kucuk K, Aryal S, Timofeeva EV, Segre CU. Nanoscale MnO_2 cathodes for Li-ion batteries: effect of thermal and mechanical processing. J Power Sources 2020;448:227374. https://doi.org/10.1016/j.jpowsour.2019.227374.
[23] Kim K, Daniel G, Kessler VG, Seisenbaeva GA, Pol VG. Basic medium heterogeneous solution synthesis of α-MnO2 nanoflakes as an anode or cathode in half cell configuration (vs lithium) of li-ion batteries. Nanomaterials 2018;8:608. https://doi.org/10.3390/nano8080608.
[24] Hashemzadeh, Mehdi Kashani Motlagh M, Maghsoudipour A. A comparative study of hydrothermal and sol–gel methods in the synthesis of MnO_2 nanostructures. J Sol-Gel Sci Technol 2009;51(2):169–74. https://doi.org/10.1007/s10971-009-1978-2.
[25] Zhou J, Yu L, Sun M, Yang S, Ye F, He J, Hao Z. Novel synthesis of birnessite-type MnO 2 nanostructure for water treatment and electrochemical capacitor. Ind Eng Chem Res 2013;52(28):9586–93. https://doi.org/10.1021/ie400577a.
[26] Sotomayor FJ, Cychosz KA, Thommes M. Characterization of micro/mesoporous materials by physisorption: concepts and case studies. Acc Mater Surf Res 2018;3: 34–50.
[27] Brock SL, Duan N, Tian ZR, Giraldo O, Zhou H, Suib SL. A review of porous manganese oxides materials. Chem Mater 1998;10:2619–28. https://doi.org/10.1021/cm980227h.
[28] Tan H, Wang S. Kinetic behavior of manganese dioxide in Li/MnO 2 primary batteries investigated using electrochemical impedance spectroscopy under nonequilibrium state. J Electrochem Soc 2014;161:A1927–32. https://doi.org/10.1149/2.0981412jes.
[29] Poyraz AS, Huang J, Cheng S, Wu L, Tong X, Zhu Y, Marschilok AC, Takeuchi KJ, Takeuchi ES. Tunnel structured α-MnO 2 with different tunnel cations (H + , K + , Ag +) as cathode materials in rechargeable lithium batteries: the role of tunnel cation on electrochemistry. J Electrochem Soc 2017;164:A1983–90. https://doi.org/10.1149/2.0911709jes.
[30] Johnson CS. Development and utility of manganese oxides as cathodes in tihium batteries. J Power Sources 2007;165:559–65. https://doi.org/10.1016/j.jpowsour.2006.10.040.
[31] Johnson CS, Dees DW, Mansuetto MF, Thackeray MM, Vissers DR, Argyriou D, Loong C-K, Christensen L. Structural and electrochemical studies of α-manganese dioxide (α-MnO_2). J Power Sources 1997;68:570–7. https://doi.org/10.1016/S0378-7753(96)02633-X.
[32] Huang X, Liu Y, Liu C, Zhang J, Noonan O, Yu C. Rechargeable aluminum–selenium batteries with high capacity. Chem Sci 2018;9:5178–82. https://doi.org/10.1039/C8SC01054D.
[33] Chen Q, Heng B, Wang H, Sun D, Wang B, Sun M, Guan S, Fu R, Tang Y. Controlled facile synthesis of hierarchical CuO@MnO_2 core–shell nanosheet arrays for high-performance lithium-ion battery. J Alloy Compd 2015;641:80–6. https://doi.org/10.1016/j.jallcom.2015.03.234.
[34] Xia H, Lai M, Lu L. Nanoflaky MnO2/carbon nanotube nanocomposites as anode materials for lithium-ion batteries. J. Mater. Chem. 2010;20:6896–902. https://doi.org/10.1039/C0JM00759E.
[35] Hu Y-S, Guo Y-G, Sigle W, Hore S, Balaya P, Maier J. Electrochemical lithiation synthesis of nanoporous materials with superior catalytic and capacitive activity. Nature Mater 2006;5(9):713–7. https://doi.org/10.1038/nmat1709.
[36] Zhou D, Zhang K, Ravey A, Gao F, Miraoui A. Parameter sensitivity analysis for fractional-order modeling of lithium-ion batteries. Energies 2016;9:123. https://doi.org/10.3390/en9030123.
[37] Quiroga-González E, Carstensen J, Föll H. Structural and electrochemical investigation during the first charging cycles of silicon microwire array anodes for high capacity lithium ion batteries. Materials 2013;6:626–36. https://doi.org/10.3390/ma6020626.